ACS PHYSICAL CHEMISTRY Au
AN OPEN ACCESS JOURNAL OF THE AMERICAN CHEMICAL SOCIETY

pubs.acs.org/physchemau
Article

Dye Modified Phenylenediamine Oligomers: Theoretical Studies on Drug Binding for Their Potential Application in Drug Sensors

Ufana Riaz* and Syed Marghoob Ashraf

Cite This: ACS Phys. Chem Au 2023, 3, 521−531
Read Online
ACCESS | Metrics & More | Article Recommendations | Supporting Information

ABSTRACT: The present work reports, for the first time, synthesis of dye incorporated *o*-phenylenediamine (OBB) with a view to obtain a conjugated oligomer with enhanced functionality. The structure was confirmed by IR studies, while the electronic transitions were confirmed by UV visible studies. The dye modified oligomer showed one order higher fluorescence intensity than the pristine Bismarck Brown (BB) dye. Confocal imaging showed red emission which could be utilized in near infra-red imaging. Density functional theory (DFT) studies were carried out to predict the theoretical properties of the oligomers. The energies of the highest occupied molecular orbital (HOMO) and the lowest unoccupied molecular orbital orbital were computed to explore how the HOMO energies of the reactants initiated the electronic interactions between them. The interaction energies were correlated to conjugation/hyper conjugation stabilization energies of the natural bond orbitals (NBO) via the DFT method using the B3LYP functional with the 6-311G(d) basis set on Gaussian 09 software. Drug binding was evaluated through simulation of interaction energy, (ΔE_{A-x}) with drugs such as captopril, propranolol, thiazide, and fentanyl. The results predicted that the oligomer could be developed into a fentanyl drug sensor.

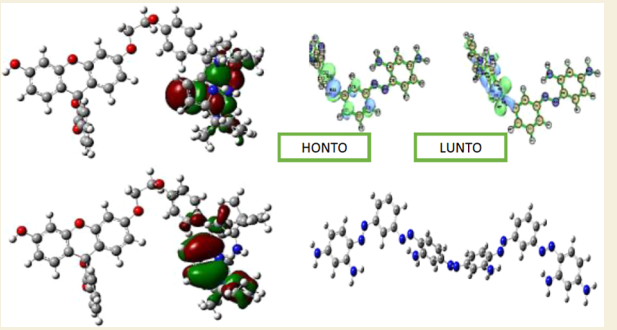

KEYWORDS: *oligomerization, fluorescence, confocal imaging, DFT studies, natural bond order*

INTRODUCTION

Conjugated polymers (CPs) have become one of the most vibrant areas of research in the field of advance functional materials due to their light weight, thermal stability, and tuneable optical properties.[1−4] The huge demand for low-cost flexible electronic devices continues to drive the development of next-generation electronic artefacts.[5] Benefitting from new structural designs and improved fabrication processes, significant progress has been made in CP synthesis leading to remarkable enhancement in optoelectronic properties such as high quantum yield and fluorescence emission in the near infrared region matching those of inorganic quantum dots.[6]

Bismarck Brown Y (BB) dye is widely used in staining of biological tissues and tanning of leather.[7] It goes as waste in the later industries which leads to water pollution.[8] Hence, if the dye could be recovered and profitably used in the synthesis of fluorescent probes, photovoltaic devices and light emitting diodes, it can not only solve the problem of water pollution but also save the cost of designing multifunctional polymers.[9,10] BB dye has three phenylene rings, two azo bonds between first/second and second/third phenylene rings, and several free amino groups that can undergo polymerization, Figure 1. The dye molecule also has twist in its structure and has long conjugation across two azo bonds.[11]

This conjugation can be further extended if the dye molecule is oligomerized with *o*-phenylenediamine and is expected to engender novel photo-physical and electronic properties.[11] In our previous studies, we have reported the polymerization of conducting polymers with dyes such as Malachite Green (MG),[12] Congo Red (CR),[13] Sudan Yellow [SY],[14] Azo benzene,[15] Amido Black 10B (AB-10B),[16] Alizarin Red (AR)[16] as well as doping of the conducting polymers with Acid Orange (AO), fluorescein (Fluo), and rhodamine-6G (R6G) dyes.[17] The application of these CPs as imaging agents has also been well-documented.[18,19]

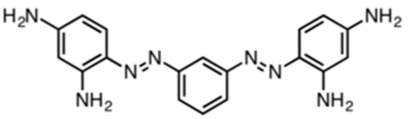

Figure 1. Structure of BB dye.

In the present study, we have laid more emphasis on the theoretical aspects of oligomerization of dyes with conducting monomers which can help in predicting the interaction of the

Received: May 28, 2023
Revised: August 9, 2023
Accepted: August 11, 2023
Published: August 28, 2023

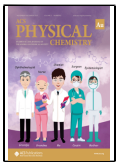

https://doi.org/10.1021/acsphyschemau.3c00025
ACS Phys. Chem Au 2023, 3, 521−531

reactants as well as their chemical stability besides their electronic characteristics. We have synthesized BB dye oligomer as well as its oligomers with *o*-phenylenediamine (OPD) in three different ratios. The oligomers were experimentally characterized by IR, UV, fluorescence spectroscopies, confocal imaging and SEM, to explore their photophysical and morphological characteristics. The theoretical properties were computed via time-dependent density functional theory (TD-DFT) using the B3LYP functional with the 6-311G(d) basis set on Gaussian 09 software for optimizing the oligomer structures and finding out highest occupied molecular orbital (HOMO)−lowest unoccupied molecular orbital (LUMO) energies and optical band gap. The conjugation/hyper-conjugation stabilization energies across the azo bond formed between BB dye and OPD molecules was computed through NBO analysis to find out which of the two molecules initiates conjugation/hyper-conjugation in the oligomer. The experimental FTIR, UV−visible studies were compared with the computationally obtained results. SEM and confocal imaging studies were carried out to analyze the morphological features and imaging capability of the oligomers. The BB/OPD-1/2 oligomer was conjugated with drugs used in heart ailments: captopril (CPT), propanolol (PPN), a diuretic drug: hydrochlorothiazide (HCTZ), and a synthetic opioid used in pain management: fentanyl (FEN) to theoretically infer their binding efficiency.

EXPERIMENTAL SECTION

Bismarck Brown Y dye (SD Fine Chem Ltd, India), *o*-phenylenediamine (Sigma-Aldrich, USA), ferric chloride (Merck, India), hydrochloric acid (Merck, India), *N*-*N* dimethyl pyrrolidone (NMP) (Merck, India), dimethyl formamide (DMF) were used without further purification. Double distilled water was used throughout the synthesis.

Oligomerization of Bismarck Brown (BB) Dye

Bismarck Brown Y (BB) (1 g, 4.6×10^{-3} mol) was dissolved in aqueous solution of 2 M HCl (25 mL). Ferric chloride (1 g, 6.17×10^{-3} mol) dissolved in distilled water (25 mL) was added to the above reaction mixture drop by drop with the help of.a burette. The reaction mixture was continuously stirred on a magnetic stirrer at −5 to 0 °C to for 2 h. After completion of the reaction, the solution was stored in deep freezer for 24 h. The obtained oligomer was then centrifuged and dried in a vacuum oven for 72 h at 70 °C and was designated as OBB.

Oligomerization of *o*-Phenylenediamine with Bismarck Brown Dye

BB dye (1 g, 4.6×10^{-3} mol) dissolved in an aqueous solution of 2 M HCl (25 mL) and *o*-phenylenediamine (0.497 g, 4.6×10^{-3} mol) dissolved in DMF (5 mL) were added to 250 mL Erlenmeyer flask. The solution was stirred at 25 °C for 20 min. Ferric chloride (1 g, 6.17×10^{-3} mol) dissolved in distilled water (25 mL) was added to the above mixture and stirred for 2 h at −5 °C. The obtained product was kept in a deep freezer for 24 h. Purified products were obtained via Soxhlet extraction using ethanol and then dried in a vacuum oven for 72 h at 70 °C to ensure complete removal of water and impurities. The oligomer was designated as BB/OPD-1/1. A similar procedure was adopted for the synthesis of oligomers BB/OPD-2/1 and BB/OPD-1/2 by varying the molar ratio of the dye/monomer.

Characterization

Spectral Measurements. IR measurements were carried out on Fourier transform infrared (FT-IR) spectrophotometer model Shimadzu IRA Affinity-1 in the form of KBr pellets. UV−visible spectra were taken on PerkinElmer-Lambda-Ez-25. Fluorescence spectra of the sample were taken in on a fluorescence spectrophotometer model Horiba Fluorolog 3-11. Viscosity average molecular weight was calculated as per the method reported in our previous studies.[17]

Morphological and Confocal Imaging Studies. SEM images were obtained on field emission-scanning electron microscope (FE-SEM), Leo Supra 50VP, Carl Zeiss, Germany, equipped with an energy-dispersive X-ray system.

DFT Studies. The computational studies were done in the gas phase using the Becke3-Lee−Yang−Parr (B3LYP) functional with the 6-311G(d) basis set on Gaussian 09W software.[20,21] The theoretically calculated FT-IR spectra were obtained at the same level of the theory. Intermolecular interaction (total and counterpoise corrected interaction energies), charge analysis (Mulliken and natural bonding orbital), and molecular orbital analysis (HOMO and LUMO), were simulated at the above-mentioned level of theory. Band gap is estimated from the difference of HOMO and LUMO energies, and it gives an idea about the change in conductivity of polymer upon interaction with different molecules. The vertical electronic excitation energies were computed by using the TD-DFT approach using the B3LYP functional and the 6-311G(d) basis set on the previously optimized molecular geometries obtained at the same level of calculation.[22,23] TD-DFT formalism provided information about excitation energies and oscillator strength values. Natural bond order (NBO) analysis gives a clear evidence of stabilization originating from hyperconjugation of various intramolecular interactions. Conjugation and hyper conjugation stabilization energies were simulated across the azo bond between BB dye and OPD, to find out which was the most reactive moiety (BB or OPD) and the direction from which the insertion of OPD proceeded (BB → OPD or OPD → BB). Natural transition orbitals (NTOs) were generated for the lowest energy transitions using Gaussian 09 software, and population analysis of the NTOs was done using the Multiwfn program.[24] The highest occupied natural transition orbital (HONTO) to the lowest unoccupied natural transition orbital (LUNTO) excitation amplitude is always the most significant for any particular excited state, due to its dominating role in determining the one electron transition for the generation of the corresponding excited state from the ground state (S_0).[24] The overlap extents between HONTO and LUNTO at S_1 (IS) and T_1 (IT) states, which take full considerations of electron transition components at the corresponding excited states, were also calculated using Multiwfn.[24]

RESULTS AND DISCUSSION

Molar Masses of the Oligomers

The mechanism of electrochemical oligomerization of BB has been well-documented in literature and was found to undergo via the azo linkages.[11] We have for the first time attempted to chemically oligomerize BB dye with OPD through the chemical oxidation method which is shown in Supporting Information as scheme S1a−c. The intrinsic viscosity (η) and viscosity average molecular weight was determined using the method reported in our previous studies.[17,18] The η values were found to be 0.32 for oligomeric OBB. The viscosity average molecular weight $\bar{M}_v$ was determined as 2192 for OBB. The η values for BB/OPD-2/1, BB/OPD-1/1, and BB/OPD-1/2 were calculated to be 0.61, 0.555, and 0.41, respectively, while the $\bar{M}_v$ values were computed to be 5891, 5090, and 4385 for BB/OPD-2/1, BB/OPD-1/1, and BB/OPD-1/2, respectively. The solubility data is given in Supporting Information as Table S1. The $\bar{M}_v$ values clearly confirmed the formation of oligomers.

Fluorescence Study of OBB Oligomer and BB/OPD Oligomers

The oligomer OBB, Figure 2, showed a fluorescence peak at 550 nm indicating a large Stokes shift of 110 nm. The peak was well formed, a Gaussian type, but had low intensity. It showed very low quantum yield and hence greater part of the emissive

https://doi.org/10.1021/acsphyschemau.3c00025
ACS Phys. Chem Au 2023, 3, 521−531

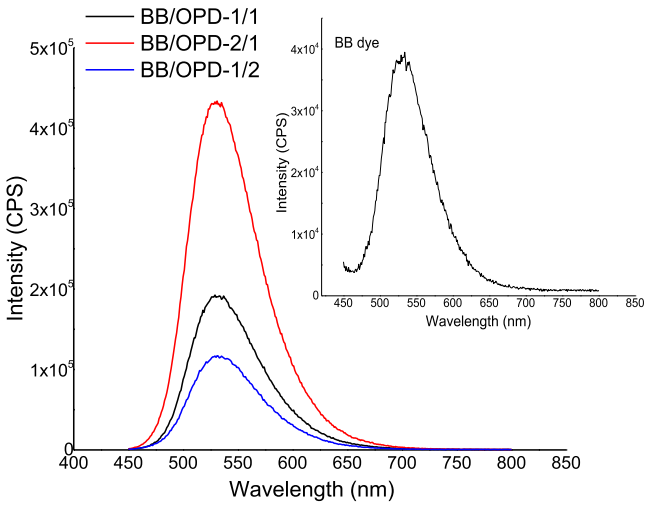

Figure 2. Fluorescence spectra of BIS-OPD oligomers.

radiation was presumably lost by the non-radiative path. It was observed that the fluorescence intensity of the three oligomers was more than 1 order of magnitude higher than the BB dye. The enhancement in the fluorescent intensity in these oligomers occurred due to aggregation induced emission (AIE).[25]

It appeared that the dye aggregation was enhanced upon oligomerization of BB with OPD which also resulted in the enhancement of the fluorescence intensity by more than an order of magnitude, Table 1. The BB/OPD-2/1 oligomer

Table 1. Fluorescence Characteristics of OBB Oligomer and BB/OPD Oligomers

sample	λ_{max}	integrated area	quantum yield (φ)
OBB	529	3 553 785	0.097
BIS-OPD-2/1	535	9 775 490	0.352
BIS-OPD-1/1	530	15 816 415	0.212
BIS-OPD-1/2	535	35 859 505	0.124

exhibited twice as higher fluorescence intensity than the BB/OPF-1/1 oligomer, while the latter has about 1.8 times higher in fluorescence intensity than the BB/OPD-1/2 oligomer. It can be inferred that in addition to the aggregation effect, the higher amount of dye in the oligomer also contributed to the fluorescence intensity which was reflected by the highest quantum yield value of 0.352 for the BB/OPD-2/1 oligomer and lowest quantum yield value of 0.124 for BB/OPD-1/2 oligomer. The planar structure of the oligomers helped in increasing the fluorescence intensity. The BB/OPD-1/1, BB/OPD-1/2, and BB/OPD-2/1 oligomers showed fluorescence peaks between 530 and 535 nm and a large blueshift of about 15 nm was observed in these oligomers. The OPD engenders aggregation induced intensity (AIE) effect in these oligomers and also blocks the torsion of the azo group, or causes restriction of intramolecular motion (RIM), in the aggregated dyes which produces blueshift in these oligomers.[25,26] A large Stokes's shift of 110 nm may have resulted from the structural difference between the ground and excited states of the oligomers.[25,26]

SEM and Confocal Images of OBB and BB/OPD Oligomers

The confocal image of pure BB, Figure 3a, revealed scant red emission from discrete particles. The particles were bulky; hence reflections were poor. BB/OPD-2/1, Figure 3b, exhibited red emission from localized regions of thick flat particles. It appears that emission emanates from the particles' ultra-thin regions, which normally occur at the boundary of the particles. The confocal image of BB/OPD-1/1, Figure 3c, showed red emission throughout the whole cross-section. In this case, the particles are relatively thin which causes the emission to be relatively uniform and a little brighter. The confocal image of BB/OPD-1/2, Figure 3d, yielded thick particles; the red emission was observed, but the emissive regions were not as prominent as in the previous case. BB-OPD-1/1 showed best red emission because of its capability to form thin particles; hence it can be used in near infra-red imaging.

The SEM of OBB, Figure 4a, showed minuscule nuggets of Bismarck joined to each other intimately forming big lumps which lay snugly to each other. The SEM of BB/OPD-2/1 Figure 4c exhibited miniscule particles larger than those in OBB which join in the same manner as in the case of OBB. In this oligomer, the effect of higher amount of BB dye is manifestly visible. The effect of higher amount of OPD in the remaining two oligomers was easily visible, Figure 4b,d. In these oligomers, minute particles joined each other intimately and made a flowery structure. The microstructures were visibly different from those of OBB and BB/OPD-2/1. When seen broadly, the microstructures of BB/OPD-1/1, Figure 4b, and BB/OPD-1/2, Figure 4d, the latter oligomer appeared brighter than the former one and agglomerates in the latter oligomer were larger than the former one. These effects could be correlated to the proportionately highest, and penultimately highest loading of OPD in the oligomer BB/OPD-1/2 and BB/OPD-1/1 respectively.

Geometry Optimization, Mulliken Charge Distribution of OBB and BB/OPD Oligomers

The geometry optimization of OBB was carried out by taking two units of the BB dye. The optimized geometries for the oligomers were computed by taking 2 units of BB dye and 1 unit of OPD for BB/OPD-2/1; 1 unit of BB dye and 1 unit of OPD for BB/OPD-1/1 and 1 unit of BB dye and 2 units of OPD for BB/OPD-1/2, respectively. The experimental as well as theoretical data were compared to confirm the proposed structure of the oligomer as well as oligomers of BB with OPD. The optimized geometries as well as Mulliken charge distribution is provided in Supporting Information as Figure S1a–d. The oligomer OBB, Figure S1a, revealed a twisted configuration around the azo linkage, while the Mulliken negative charge in OBB was noticed to be concentrated around the nitrogen atoms of the amino group as well as the nitrogen of azo linkages. The optimized geometries of BB/OPD-2/1, BB/OPD-1/1, and BB/OPD-1/2, showed planar configuration with negative charges concentrated around the nitrogen of amino as well as azo linkages (given in Supporting Information as Figure S1b–d). It also showed distribution of a partial negative charge on carbons in OBB and BB/OPD-2/1, BB/OPD-1/1 and BB/OPD-1/2, respectively.

Experimental and Theoretical IR Analyses of OBB Oligomer and BB/OPD Oligomer

The IR spectral data of OBB and its oligomers are given in Table 2, while the actual spectra are compiled in Supporting Information as Figure S2a–d. The spectrum of OBB revealed an N–H stretching vibration peak at 3355 cm^{-1} due to the presence of secondary amine (–NH). The area under the peak

https://doi.org/10.1021/acsphyschemau.3c00025
ACS Phys. Chem Au 2023, 3, 521–531

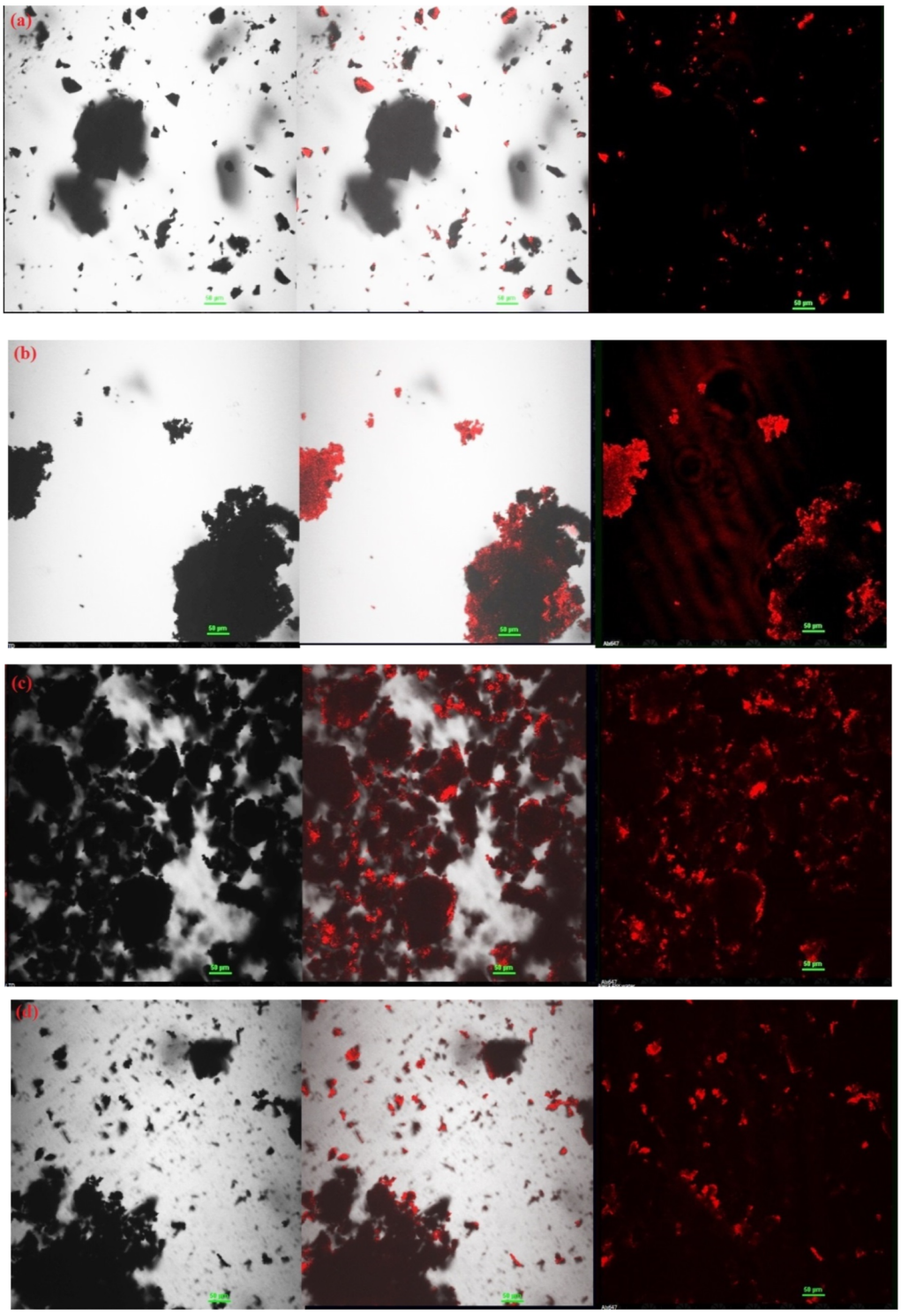

Figure 3. Confocal images of (a) OBB, (b) BB/OPD-2/1, (c) BB/POPD-1/1, and (d) BB/POPD-1/2.

was calculated to be 586.6 cm^{-1}. The imine bending peak was noticed at 1610 cm^{-1}. The peak at 1326 cm^{-1} was designated to ring puckering of benzenoid rings. The copolymer of BB/OPD-2/1 revealed a NH stretching peak at 3120 cm^{-1}. The NH peak shifted to lower wavenumbers. Similarly, the NH stretching peak for BB/OPD-1/1 was found at 3100 cm^{-1}, while for BB/OPD-1/2, it was noticed at 3100 cm^{-1}. With the increasing ratio of BB, small change in the NH peak values in oligomers was noticed. It confirmed the interaction between BB and OPD.

Values of the IR peaks of different functional groups and chemical bonds, given as second column in Table 2, were computed by DFT studies. The peak values computed theoretically closely match their corresponding experimental values. This validates the theoretical protocol followed by us.

Analysis of Frontier Molecular Orbitals of Oligomers

Frontier molecular orbitals of BB/OPD-1/1, BB/OPD-2/1, and BB/OPD-1/2 oligomers are depicted in Figure 5a–c. The BB/OPD-1/1 oligomer, Figure 5a, yielded a band gap of 3.24

https://doi.org/10.1021/acsphyschemau.3c00025
ACS Phys. Chem Au 2023, 3, 521–531

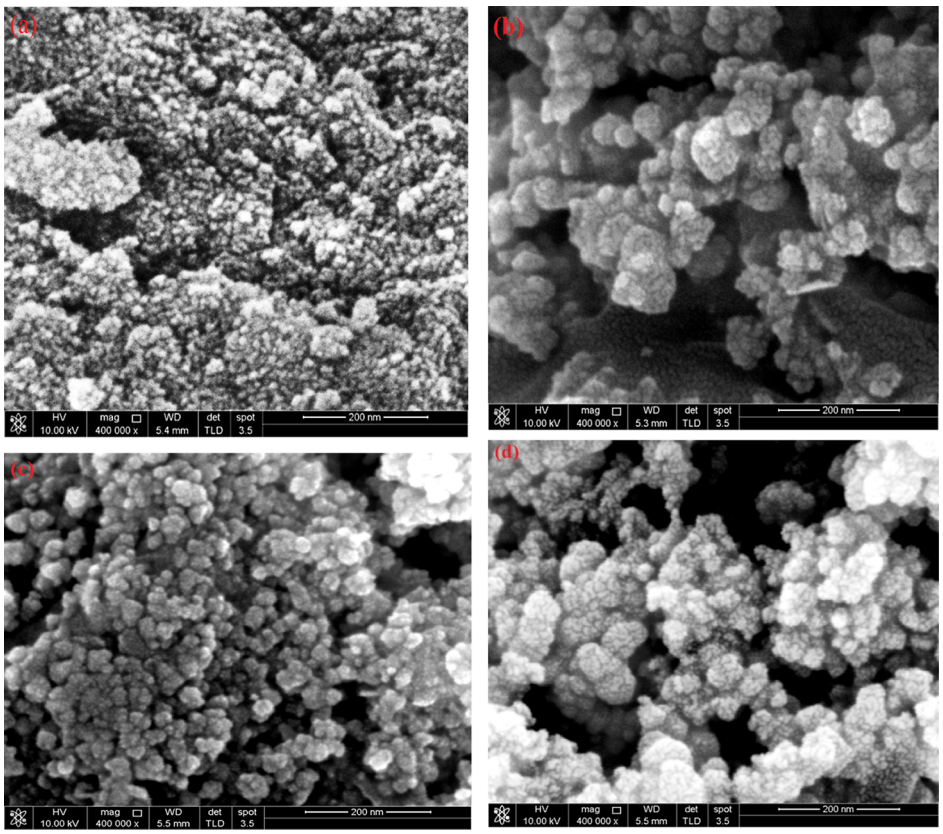

Figure 4. SEM images of (a) OBB, (b) BB/OPD-1/1, (c) BB/OPD-2/1, and (d) BB/OPD-1/2.

Table 2. IR Data of OBB and BB/OPD Oligomers

samples	functional group	wavenumber/(cm^{-1})experimental	wavenumber/(cm^{-1}) theoretical
OBB	N−H stretching	3355	3350
	imine (C═N)	1610	1620
	C═C stretching (benzenoid)	1326	1350, 1320
	C−N bending	1234	1230
	C−H bending	1110	1120, 1110
	substituted benzene ring	995	990, 930
BB/OPD-2/1	N−H stretching	3120	3110
	imine (C═N)	1608	1630
	C═C stretching (benzenoid)	1373	1370, 1320
	C−N bending	1263	1260, 1220
	C−H bending	1118, 1054	1120, 1060
	p-substituted benzene ring	833, 792	950, 880
	aromatic ring of POPD	730, 599	790, 600, 590
BB/OPD-1/2	N−H stretching	3100	3100
	imine (C═N)	1610	1615
	C═C stretching (benzenoid)	1344	1340
	C−N bending	1221	1220
	C−H bending	1039	1040
	p-substituted benzene ring	910	910
	aromatic ring of POPD	730, 599	790, 600, 590
BIS-OPD-1/1	N−H stretching	3100	3100
	N−H stretching	3090	3090
	imine (C═N)	1612	1600
	C═C stretching (benzenoid)	1326	1380, 1376, 1320
	C−N bending	1236	1230
	C−H bending	1051	1050
	p-substituted benzene ring	825	820, 800
	aromatic ring of POPD	736	730, 700

https://doi.org/10.1021/acsphyschemau.3c00025
ACS Phys. Chem Au 2023, 3, 521−531

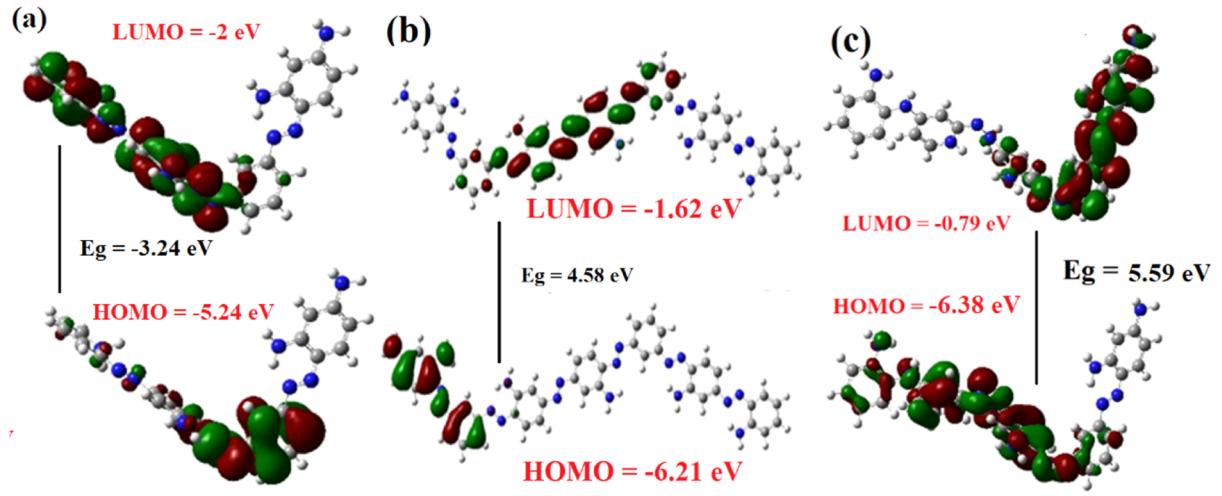

Figure 5. Frontier molecular orbitals of (a) BB/OPD-1/1, (b) BB/OPD-2/1, and (c) BB/OPD-1/2.

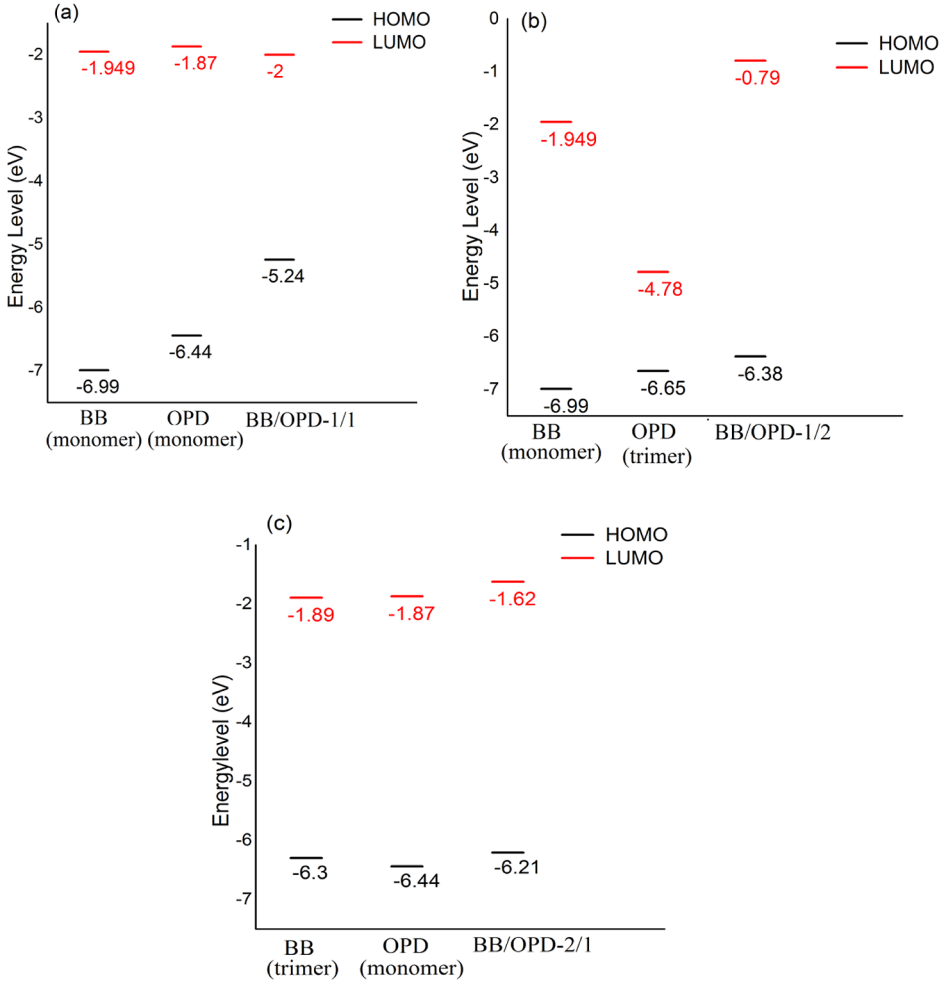

Figure 6. HOMO−LUMO energies of OPD, BB, and their oligomers (a) BB/OPD-1/1, (b) BB/OPD-1/2, and (c) BB/OPD-2/1.

eV. This can be called a poor semiconductor. The HOMO orbitals were noticed to be concentrated in the area near the end of the BB unit, while the LUMO orbitals were found to be spread over first two benzene rings wholly, leaving only the last benzene ring. DFT calculations revealed overlap integral as 0.5342 (53.4%). This also indicated a lower band gap and intra-molecular charge transfer. The oligomer BB/OPD-2/1, Figure 5b, exhibited a band gap of 4.58 eV. It showed that the oligomer was an insulator. The HOMO orbital was noticed to be concentrated on the first two rings of the BB moiety. The structure also revealed that the HOMO charge density was low. LUMO was found to occupy the third, fourth, and fifth benzene rings of the BB unit. LUMO charge density appeared to be quite low. The overlap of orbitals also appeared to be

https://doi.org/10.1021/acsphyschemau.3c00025
ACS Phys. Chem Au 2023, 3, 521−531

low. The DFT calculations exhibited an overlap integral value equal to 0.0590 (5.9%), which was also quite low. The oligomer BB/OPD-1/2, Figure 5c, showed a band gap value of 5.59 eV. This showed that the oligomer was a good insulator. The HOMO orbitals were found to be spread partly over the first benzene ring and fully over the second and third benzene ring as well as partly on one benzene ring of OPD. The structure revealed that the HOMO charge density was high only on the second and third benzene units of BB. The LUMO orbitals were concentrated over the two benzene units of OPD and third benzene unit of BB with high LUMO charge density. The overlap of orbitals appeared to be fair, while the DFT calculations showed a matching overlap integral value equal to 0.3723 (37.23%). The high band gap of this oligomer matched with those of diamond (5.46 eV),[27] polystyrene (4.4 eV),[28] poly(methyl methacrylate) (5.6 eV),[29] polyethylene terephthalate (4.0 eV),[30] and poly(tetrafluoro ethylene) (5.37 eV).[31] It was found to be only two odd units less than the highest organic insulator polyethylene and polypropylene. This oligomer, therefore, shows promise to be used as a gate insulator in OFETs and also as a Schottky diode.

Comparison of HOMO−LUMO Energies of OPD, OBB, and Their Oligomers

The energies of HOMO and LUMO orbitals of OPD, BB, and the three sets of oligomers in different ratios of OPD and BB were compared to reveal the relative stability of oligomers. Figure 6a shows HOMO−LUMO energy levels of OPD (monomer), BB (monomer), and BB/OPD-1/1 oligomer, Figure 6b, represents HOMO−LUMO energy levels of OPD (trimer), BB (monomer), and -BB/OPD-1/2 oligomer, while Figure 6c exhibits HOMO−LUMO energy levels of OPD (monomer), BB (dimer), and BB/OPD-2/1 oligomer. Figure 6a revealed that the HOMO energy level of the oligomer BB/OPD-1/1, occurred at −5.2 eV compared to that of OPD (−6.4 eV) and BB (−7.0 eV). This establishes the reaction of OPD with BB and that the oligomer to be less stable than individual OPD and BB monomers. The formation of this oligomer was stabilized through a high stabilization energy of 1466 kcal of natural bond order (NBO). This energy is calculated in the next section. The LUMO energy values of OPD (−1.87 eV) and BB (−1.94 eV) stabilized the LUMO energy value of the oligomer BB/OPD-1/1 to −2.0 eV which also contributed to the stabilization of this oligomer.

The oligomer BB/OPD-1/2, wherein the ratio of BB to OPD is 1/2, Figure 6b, OPD dimer revealed an unexpected value of HOMO energy level (not shown). The HOMO energy value of the OPD trimer looked reasonable being −6.65 eV, but the LUMO energy level appeared to be far deeper being −4.78 eV showing very low tendency of accepting electrons. BB carried a HOMO energy value of −6.99 eV and LUMO energy value of −1.94 eV, the former value showing strong electron donor capacity. Upon interaction of OPD dimer (trimer) and BB monomer, the HOMO energy value of BB/OPD-1/2 occurred at −6.38 eV. This showed fairly strong interaction between two reactants in the given proportion. This was also supported by fairly high value of NBO stabilization energy of the oligomer being 1200 kcal. The LUMO energy level of the oligomer occurred at −0.79 eV. This indicated that the oligomer was a good electron acceptor and could be easily reduced. Since the OPD dimer gives erratic values, it can be deduced that it is not the OPD dimer that reacts with the BB, but it is the two OPD monomers reacting with the BB individually one after another. In the oligomer, BB/OPD-2/1, Figure 6c, BB (dimer) HOMO energy level was observed to be −6.3 eV, OPD (monomer) energy value was found to be −6.4 eV which caused the HOMO energy value of BB/OPD−OPD 2/1 to have a value of −6.21 eV. The HOMO energy values of the two reactants were found to be quite close to each other (−6.3 and −6.4 eV) indicating low electronic interaction between OPD and BB. The HOMO energy value of the oligomer (−6.21 eV) was observed slightly above the reactants. This indicated low stabilization energy of the oligomer. It was observed that the oligomer was stabilized by a low NBO stabilization energy of 659 kcal. Even LUMO energy levels of the OPD and BB were computed to be quite close to each other, being −1.87 and 1.89 eV, respectively, causing the LUMO energy value to go slightly above them to −1.62 eV, Figure 6b. This confirmed the low LUMO electronic interaction between the moieties and the less stabilized LUMO energy of the oligomer matched with the low NBO stabilization energy of the oligomer (659 kcal).

DFT Calculation of Conjugation/Hyper-conjugation Stabilization Energies of NBOs from BB to OPD and OPD to BB across Intervening Azo Bonds

We have calculated the conjugation/hyper-conjugation stabilization energies of NBOs across the azo bond between BB and OPD (BB ↔ OPD) in all three cases of oligomer formation using the B3LYP functional with the 6-311G(d) basis set. In the system, BB/OPD-1/2 (given in Supporting Information as Tables S2−S4), the sum of hyper-conjugation/conjugation stabilization energy of NBOs from BB → OPD was found to be 3832 kcal/mol, while the same from OPD → BB was obtained as 2632 kcal/mol. The difference between the two sides of conjugation/hyper-conjugation energies of NBOs, BB ↔ OPD, was found to be 1200 kcal. Thus, the stabilization of the BB-OPD oligomer occurred through higher conjugation/hyper-conjugation energies of NBOs from BB to OPD. It reveals BB is more reactive than OBB.

In the system BB/OPD-2/1 (given in Supporting Information as Table S4), the conjugation/hyper conjugation energies of NBOs from BB → OPD was higher by 659 kcal/mol than the same from OPD → BB. The conjugation/hyper-conjugation energies of NBOs from BB ↔ OPD were, respectively, 4812 and 4153 kcal/mol. It reveals that reaction occurs in the direction BB → OPD, in other words BB is more reactive than OPD. Comparing the stabilization energies of complexes BB/OPD-2/1 and BB/OPD-1/2, the latter is found to be more stable than the former. The oligomer BB/OPD-1/1 exhibited the individual/hyper-conjugation energies of each direction of NBOs, BB ↔ OPD, as 8403 and 6937 kcal/mol, higher than the corresponding energy values in the preceding two systems (given in Supporting Information as Table S2). The net stabilization energy of this system, $\Delta E_{(BB\rightarrow OPD-OPD\rightarrow BB)}$ of BB/OPD-1/1, was obtained as 1466 kcal/mol. Comparing the $\Delta E_{(BB\rightarrow OPD-OPD\rightarrow BB)}$ values, it can be concluded that the system BB/OPD-1/1 was the highest in stability, while the system BB-OPD-2/1 was computed to have the lowest in stability. It was also observed that individual conjugation/hyper-conjugation NBO energies were controlled by the amount of BB in the oligomer. In the oligomer BB-OPD-1/2, the individual NBO energies varied between 367 and 401 kcal/mol. In the system BB-OPD-2/1, the lowest value of the NBO energy was 573 kcal/mol and highest was 605 kcal/mol, while the system BB-OPD-1/1 (2/2) showed

https://doi.org/10.1021/acsphyschemau.3c00025
ACS Phys. Chem Au 2023, 3, 521−531

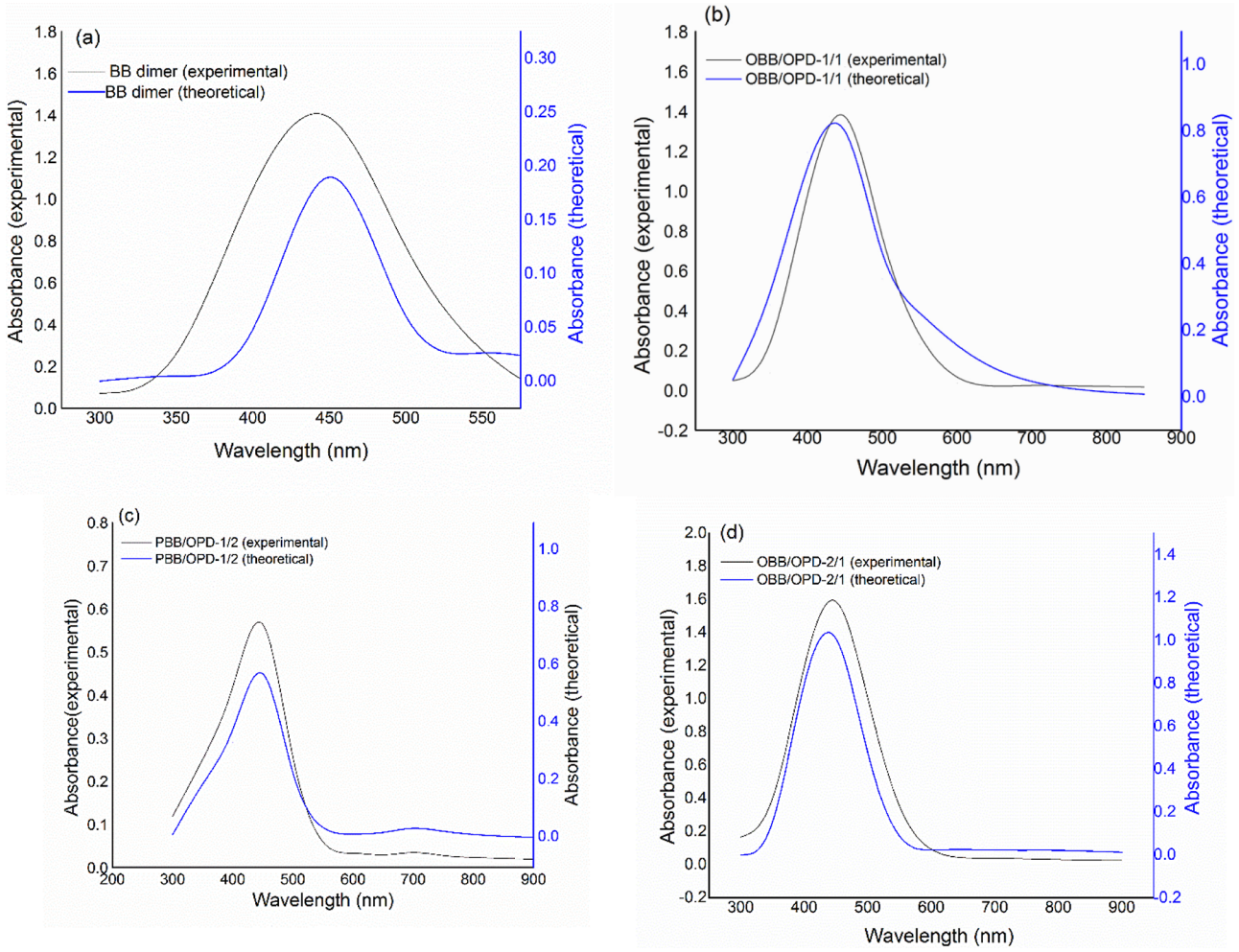

Figure 7. UV visible spectra of (a) OBB, (b) BB/OPD-1/1, (c) BB/OPD-1/2, and (d) BB/OPD-2/1.

the lowest NBO energy as 556 kcal/mol and highest value as 666 kcal/mol. The results of the NBO stabilization energies match with those of HOMO−LUMO energies.

Comparison of Experimental and Theoretical UV−Visible Spectra and Analysis of Electronic Transitions

Theoretical spectra of OBB, Figure 7a, calculated through TD-DFT revealed a peak at 450 nm; the experimental value of this peak was found to be the same. The theoretical and experimental values are closely matching. The peak arises due to n−π^* transition. The theoretical value of oscillator strength was computed to be 1.4 for this peak, while the experimental value was found to be 0.88. These values are also matching as given in Table 3. The experimental and theoretical values of the transition peak for the oligomer BB/OPD-1/1, Figure 7b, were found to be 450 nm. The experimental and theoretical peak values of the oligomer BB/OPD-1/2 are 450 and 448 nm, Figure 7c. The difference in the two values is noticeable. If the theoretical protocol is further improved, the two values could be matching. This also confirms the validity of our theoretical protocol. The oligomer BB/OPD-2/1 Figure 7d showed the experimental and theoretical peak values as 450 and 447 nm, respectively. The experimental value of the transition peak was the same in the three cases, since it emanates from the azo group, extended conjugation does not affect this value. Absorption intensity is the highest in the case of BB/OPD-2/1 (1.55), followed by BB/OPD-1/1 (1.35), and the lowest in the case of BB/OPD-1/2 (0.55). The absorption intensity depended on the azo bond unit per mol which is the highest in BB/OPD-2/1, followed by BB/OPD-1/1, and the lowest in BB/OPD-1/2 which matches with the molar masses of the oligomers (viz., section Molar Masses of Oligomers).

Oscillator strength values were found to noticeably decrease with the increase in the loading of OPD in BB. The oscillator strength value of BB/OPD-2/1(0.23/0.25) was found higher than that of other two oligomers with values 1.6, 0.16 and 0.17 respectively, Table 3. This occurs due the decrease in transition dipole moment intensity which depends on the value of q and r evident from HONTO−LUNTO orbitals, the same being highest in the oligomer BB/OPD-2/1, (given in Supporting Information as Figure S3a−c).

Table 3. UV−Visible spectra of OBB and BB/OPD Oligomers

oligomer	λ_{max} experimental (theoretical)	oscillator strength experimental (theoretical)
OBB	445 (450)	0.88 (0.94)
BIS-OPD-2/1	450 (447)	0.23 (0.25)
BIS-OPD-1/1	450 (450)	0.16 (0.15)
BIS-OPD-1/2	450 (448)	0.17 (0.16)

https://doi.org/10.1021/acsphyschemau.3c00025
ACS Phys. Chem Au 2023, 3, 521−531

Sensing of Drugs

Some authors[31−34] working on theoretical estimation of the sensing ability of several semiconductors have observed that the interaction energy of 40 kJ/mol or as low as 20 kJ/mol, of the semiconductor with the analytes ensured the sensing efficiency of the semiconductor. Apart from the interaction energy, the bandgap difference between the dye−semiconductor conjugate A, and conjugate A−drug complex and their HOMO−LUMO energy values also plays a role in sensing evaluation. These inferences have been attempted to be strengthened from the UV−visible spectral analysis. We have used the B3LYP functional with the 6-311G(d) basis set to simulate binding/interaction and HOMO−LUMO energies of these moieties to obtain information about the sensing ability of BB/OPD-1/2 for drugs like captopril, thiazide, propranolol, and fentanyl. The interaction energies (ΔE_{A-x}, E_A, and E_x) where A is the dye−semiconductor conjugate (BB/OPD-1/2) and x is the drug molecule: captopril (CPT), thiazide (HCTZ), propranolol (PPN), and fentanyl (FEN) are compiled in the Table 4.

Table 4. Energy Parameters of Dye-Oligomer−Drug Conjugate

oligomer−drug	$\Delta E_{BB/OPD-1/2-drug}$ (kcal mol^{-1})	E_{HOMO} (eV)	E_{LUMO} (eV)	band gap
BB/OPD-1/2		−6.38	−0.79	5.59
BB/OPD-1/2−CPT	−20.62	−4.11	−2.30	1.8
BB/OPD-1/2−FEN	+423	−7.31	−6.25	1.06
BB/OPD-1/2−HCTZ	−20.00	−4.41	−2.35	2.06
BB/OPD-1/2−PPN	−11.87	−4.18	−2.07	2.11

The data in the Table 4 reveals that the interaction energy $\Delta E_{BB/OPD-1/2-CPT}$ and $\Delta E_{BB/OPD-1/2-HCTZ}$ exhibit a high interaction energy of −20 kcal/mol which ensure high sensing ability of the BB/OPD-1/2 for these drugs. $\Delta E_{BB/OPD-1/2-PPN}$ is −11.875 kcal/mol which is equivalent to 49.88 kJ/mol that indicates good sensing ability of the conjugate moiety, BB/OPD-1/2 for this drug, $\Delta E_{BB/OPD-1/2-FEN}$ has an excessively high value of 400 kcal/mol; the reaction is indicated to be also endothermic. It shows this reaction occurs partly or fully using its own internal energy which will cause major electronic and structural changes in this conjugate complex. This is confirmed by excessive changes in the HUMO and LUMO energies of this conjugate complex as compared to other conjugate complexes (Table 4). The band gap of BB/OPD-1/2 is 5.59 eV. On interaction with drug captopril, the band gap decreases to 1.8 eV. A fall of 3.79 eV in the band gap value indicates a strong interaction between the conjugate BB/OPD-1/2−CPT which is reflected in noticeable change in its electronic and physical properties that can be used in sensing this drug. Likewise, the interaction of drugs thiazide and propranolol with oligomer brings down the band gap energy of conjugate BB/OPD-1/2 from 5.59 to 2.06 and 2.11 eV, respectively. Such a large fall in band gap energy of conjugate BB/OPD-1/2 is expected to reflect in good change in some of its physical or electronic properties which can be sensed with an appropriate sensor. Drug fentanyl shows a large fall from 5.5 to 1.06 eV upon interaction with the oligomer. This is the largest fall in band gap energy among these drugs. Moreover, E_{HOMO} and E_{LUMO} of the BB/OPD-1/2−FEN conjugate is, respectively, −7.31 and −6.25 eV which have strangely low values of E_{HOMO} and E_{LUMO} compared to the other three drugs (Table 4). These values indicate excessively large electronic reorganization in the BB/OPD-1/2−FEN conjugate matching with its large endothermic interaction energy. These factors favor the conjugate BB/OPD-1/2 to be potentially a good candidate for sensing these drugs. These electronic effects are revealed in the simulated UV−vis spectra of BB/OPD-1/2−drug conjugates. The conjugate BB/OPD-1/2 has a simulated UV−vis spectral peak at 420 nm. The simulated UV−vis spectral peak of BB/OPD-1/2−CPT is observed at 400 nm showing a high blueshift of 28 nm and another well-formed transition peak at 748 nm. The conjugate BB/OPD-1/2−PPN gives a main simulated UV−vis peak at 405 nm revealing a high blueshift of 43 nm. This conjugate gives an additional transition simulated peak at 648 nm. The conjugate BB/OPD-1/2−HCTZ shows the main simulated transition peak at 430 nm giving a blueshift of 18 nm and another well-formed simulated peak at 650 nm. The conjugate BB/OPD-1/2−FEN exhibits the main simulated transition peak at 530 nm giving a huge redshift of 82 nm matching with its endothermic property, opposed to the blueshift given by other three drugs. This conjugate does not reveal a second transition peak. Although we have not given the simulated energy parameter of BB/OPD-1/2−ATN, its simulated UV−vis spectra give a main transition peak at 400 nm and the second transition peak at 615 nm of high transition intensity. The above results reveal that taking into account the differently located two transitional peaks, their peak values and intensity of the conjugates BB/OPD-1/2−CPT, BB/OPD-1/2−PPN, BB/OPD-1/2−HCTZ, and BB/OPD-1/2−ATN and the peak value and the peak intensity of hugely redshifted conjugate BB/OPD-1/2−FEN a sensor can be developed for these drugs. Our studies on the electrochemical sensing of drugs using BB/OPD-1/2 are underway and will be published soon.

CONCLUSIONS

Oligomers of BB with OPD were successfully synthesized. The HOMO−LUMO energies of the three oligomers reveal highest stability of the oligomer BB/OPD-1/1 which is also confirmed by highest conjugation/hyper-conjugation NBO stabilization energy of this oligomer. UV−vis spectra revealed that the oligomer BB/OPD-2/1 showed the highest optical absorption intensity. The absorption intensity of these oligomers depends upon the number of azo bonds per gram mol. Fluorescence studies revealed that the oligomers showed one order higher fluorescence intensity than the OBB oligomer through aggregation-induced emission (AIE) mechanism; BB/OPD-1/1 emits brightest red emission in confocal imaging. This oligomer can be used in infrared imaging. The oligomer BB/OPD-1/2 has high insulator strength with a band gap value of 5.9 eV with a potential to be used in OFET as a gate material. The simulated electronic energies and UV−vis spectral analysis of the conjugates BB/OPD-2/1−CAPT, BB/OPD-2/1−PPN, BB/OPD-2/1−HTCZ, BB/OPD-2/1−ATEN, and BB/OPD-2/1−FEN have revealed that the conjugate BB/OPD-2/1 can be developed into an effective sensor of these drugs.

ASSOCIATED CONTENT

Supporting Information

The Supporting Information is available free of charge at https://pubs.acs.org/doi/10.1021/acsphyschemau.3c00025.

Mechanism of co-oligomerization of BB dye with OPD, optimized geometry and Mulliken charge distribution of

https://doi.org/10.1021/acsphyschemau.3c00025
ACS Phys. Chem Au 2023, 3, 521−531

OBB, BB/OPD-2/1, BB/OPD-1/1, and BB/OPD-1/2, IR spectra of OBB, BB/OPD-2/1, BB/OPD-1/1, and BB/OPD-1/2, HONTO−LUNTO orbitals of BB/OPD-1/1, BB/OPD-1/2, and BB/OPD-2/1, solubility of OBB and BB/OPD oligomers, conjugation/hyper conjugation stabilization energies of the NBOs system: BB/OPD-1/1, conjugation/hyper conjugation stabilization energies of the NBOs system: BB/OPD-1/2, and conjugation/hyper conjugation stabilization energies of the NBOs system: BB/OPD-2/1 (PDF)

AUTHOR INFORMATION

Corresponding Author

Ufana Riaz − *Department of Chemistry and Biochemistry, North Carolina Central University, Durham, North Carolina 27707, United States; Materials Research Laboratory, Department of Chemistry, Jamia Millia Islamia, New Delhi 110025, India;* orcid.org/0000-0001-7485-4103; Email: uriaz@nccu.edu, ufana2002@yahoo.co.in

Author

Syed Marghoob Ashraf − *Materials Research Laboratory, Department of Chemistry, Jamia Millia Islamia, New Delhi 110025, India*

Complete contact information is available at: https://pubs.acs.org/10.1021/acsphyschemau.3c00025

Notes

The authors declare no competing financial interest.
[§]Now retired.

ACKNOWLEDGMENTS

U.R. acknowledges the National Science Foundation (award no. 2122044) and the NSF PREM for Hybrid Nanoscale Systems between NCCU and Penn State for providing financial assistance.

REFERENCES

(1) Chen, Xi.; Hussain, S.; Abbas, A.; Hao, Y.; Malik, A. H.; Tian, X.; Song, H.; Gao, R. Conjugated polymer nanoparticles and their nanohybrids as smart photoluminescent and photo-responsive material for biosensing, imaging, and theranostics. *Microchim. Acta* **2022**, *189*, 83.

(2) Kang, S.; Kim, G.-H.; Park, S.-J. Conjugated Block Copolymers for Functional Nanostructures. *Acc. Chem. Res.* **2022**, *55*, 2224−2234.

(3) Lan, L.; Chen, J.; Wang, Y.; Li, P.; Yu, Y.; Zhu, G.; Li, Z.; Lei, T.; Yue, W.; McCulloch, I. Facilely Accessible Porous Conjugated Polymers toward High-Performance and Flexible Organic Electrochemical Transistors. *Chem. Mater.* **2022**, *34*, 1666−1676.

(4) Wang, J.; Zhu, W.; Zhang, Y.; Yang, X.; Bai, G.; Zhang, Q.; Chen, Y.; Lan, X. Structural Engineering of Donor−π−Acceptor Conjugated Polymers for Facilitating Charge Separation: A Dual-Functional Photocatalysis. *Macromolecules* **2022**, *55*, 10842−10853.

(5) Shimamura, T.; Kobayashi, A.; Oaki, Y.; Yoshida, M.; Kato, M. Water Reduction Photocathodes Based on Ru Complex Dyes Covered with a Conjugated Polymer Nanosheet. *Energy Fuels* **2022**, *36*, 11559−11566.

(6) Xu, C.; Wang, Z.; Dong, W.; He, C.; Shi, Y.; Bai, J.; Zhang, C.; Gao, M.; Jiang, H.; Deng, Y.; Ye, L.; Han, Y.; Geng, Y. Aggregation Behavior and Electrical Performance Control of Isoindigo-Based Conjugated Polymers via Carbosilane Side Chain Engineering. *Macromolecules* **2022**, *55*, 10385−10394.

(7) Ganjoo, R.; Verma, C.; Kumar, A.; Quraishi, M. A. Colloidal and interface aqueous chemistry of dyes: Past, present and future scenarios in corrosion mitigation. *Adv. Colloid Interface Sci.* **2023**, *311*, 102832.

(8) Edwards, K. E. K.; Mermut, O.; Pietro, W. J.; Barrett, C. J. Optical and computational study of the trans ↔ cis reversible isomerization of the commercial bis-azo dye Bismarck Brown Y. *Phys. Chem. Chem. Phys.* **2023**, *25*, 5673−5684.

(9) Silva, L. P. A.; Neto, J. L.; Santos, A. P. L. A.; da Silva, A. J. C.; Lima, D. J. P.; Ribeiro, A. S. A yellow to magenta multielectrochromic, pH sensor polymer based on 2,5-di(thienyl)pyrrole modified with methyl orange azo dye. *Synth. Met.* **2023**, *292*, 117241.

(10) Male, U.; Shin, B. K.; Huh, D. S. Synthesis and Characterization of Polyaniline-Grafted CNT as Electrode Materials for Supercapacitors. *Macromol. Res.* **2017**, *25*, 1121−1128.

(11) Teixeira, M. F. S.; Barsan, M. M.; Brett, C. M. A. Molecular engineering of a π-conjugated polymer film of the azo dye Bismarck Brown Y. *RSC Adv.* **2016**, *6*, 101318−101322.

(12) Riaz, U.; Singh, N. Facile synthesis of malachite green incorporated conducting polymers: A comparison of theoretical and experimental studies. *Synth. Met.* **2019**, *257*, 116184.

(13) Singh, N.; Kumar, P.; Kumar, R.; Aazam, E. S.; Riaz, U. Development of a near infrared novel bioimaging agent *via* co-oligomerization of Congo Red with aniline and *o*-phenylenediamine: experimental and theoretical studies. *RSC Adv.* **2019**, *9*, 36479−36491.

(14) Singh, N.; Ali, R.; Ashraf, S.; Rub, A.; Riaz, U. Experimental and computational studies of novel Sudan-I dye modified conjugated oligomers: Efficient $^1O_2$ generation and antileishmanial characteristics. *Mater. Sci. Eng., B* **2021**, *265*, 114993.

(15) Singh, N.; Arish, M.; Kumar, P.; Rub, A.; Riaz, U. Experimental and Theoretical Studies of Novel Azo Benzene Functionalized Conjugated Polymers: *In-vitro* Antileishmanial Activity and Bioimaging. *Sci. Rep.* **2020**, *10*, 57.

(16) Singh, N.; Kumar, P.; Kumar, R.; Riaz, U. Ultrasound-Assisted Polymerization of Dyes with Phenylenediamines: Facile Method To Design Polymeric Photosensitizers with Enhanced Singlet Oxygen Generation Characteristics and Anticancer Activity. *Ind. Eng. Chem. Res.* **2019**, *58*, 14044−14057.

(17) Riaz, U.; Ashraf, S. M.; Fatima, T.; Jadoun, S. Tuning the spectral, thermal and fuorescent properties of conjugated polymers via random copolymerization of hole transporting monomers. *Spectrochim. Acta, Part A* **2017**, *173*, 986−993.

(18) Riaz, U.; Jadoun, S.; Kumar, P.; Arish, M.; Rub, A.; Ashraf, S. M. Influence of Luminol Doping of Poly(*o*-phenylenediamine) on the Spectral, Morphological, and Fluorescent properties: A Potential Fluorescent Marker for Early detection and Diagnosis of *Leishmania donovani*. *ACS Appl. Mater. Interfaces* **2017**, *9*, 33159−33168.

(19) Tuncel, D.; Demir, H. V. Conjugated polymer nanoparticles. *Nanoscale* **2010**, *2*, 484−494.

(20) Lee, C.; Yang, W.; Parr, R. G. Development of the Colle-Salvetti correlation-energy formula into a functional of the electron density. *Phys. Rev. B: Condens. Matter Mater. Phys.* **1988**, *37*, 785−789.

(21) Frisch, M. J.; Trucks, G. W.; Schlegel, H. B.; Scuseria, G. E.; Robb, M. A.; Cheeseman, J. R.; Scalmani, G.; Barone, V.; Mennucci, B.; Petersson, G. A.; Nakatsuji, H.; Caricato, M.; Li, X.; Hratchian, H. P.; Izmaylov, A. F.; Bloino, J.; Zheng, G.; Sonnenberg, J. L.; Hada, M.; Ehara, M.; Toyota, K.; Fukuda, R.; Hasegawa, J.; Ishida, M.; Nakajima, T.; Honda, Y.; Kitao, O.; Nakai, H.; Vreven, T.; Montgomery, J. A., Jr.; Peralta, J. E.; Ogliaro, F.; Bearpark, M.; Heyd, J. J.; Brothers, E.; Kudin, K. N.; Staroverov, V. N.; Kobayashi, R.; Normand, J.; Raghavachari, K.; Rendell, A.; Burant, J. C.; Iyengar, S. S.; Tomasi, J.; Cossi, M.; Rega, N.; Millam, J. M.; Klene, M.; Knox, J. E.; Cross, J. B.; Bakken, V.; Adamo, C.; Jaramillo, J.; Gomperts, R.; Stratmann, R. E.; Yazyev, O.; Austin, A. J.; Cammi, R.; Pomelli, C.; Ochterski, J. W.; Martin, R. L.; Morokuma, K.; Zakrzewski, V. G.; Voth, G. A.; Salvador, P.; Dannenberg, J. J.; Dapprich, S.; Daniels, A. D.; Farkas, O.; Foresman, J. B.; Ortiz, J. V.; Cioslowski, J.; Fox, D. J. *Gaussian 09*, Revision A.02; Gaussian, Inc.: Wallingford CT, 2009.

(22) Bauernschmitt, R.; Ahlrichs, R. Treatment of electronic excitations within the adiabatic approximation of time dependent density functional theory. *Chem. Phys. Lett.* **1996**, *256*, 454−464.
(23) Bibi, S.; Ullah, H.; Ahmad, S. M.; Ali Shah, A. u. H.; Bilal, S.; Tahir, A. A.; Ayub, K. Molecular and Electronic Structure Elucidation of Polypyrrole Gas Sensors. *J. Phys. Chem. C* **2015**, *119*, 15994−16003.
(24) Lu, T.; Chen, F. Multiwfn: a multifunctional wavefunction analyzer. *J. Comput. Chem.* **2012**, *33*, 580−592.
(25) Sánchez-Ruiz, A.; Sousa-Hervés, A.; Tolosa Barrilero, J.; Navarro, A.; Garcia-Martinez, J. C. Aggregation-Induced Emission Properties in Fully π-Conjugated Polymers, Dendrimers, and Oligomers. *Polymers* **2021**, *13*, 213.
(26) Li, Y.; Liu, S.; Han, T.; Zhang, H.; Chuah, C.; Kwok, R. T. K.; Lam, J. W. Y.; Tang, B. Z. Sparks fly when AIE meets with polymers. *Mater. Chem. Front.* **2019**, *3*, 2207−2220.
(27) Hu, M.; Pan, Y.; Luo, K.; He, J.; Yu, D.; Xu, B. Three dimensional graphdiyne polymers with tunable band gaps. *Carbon* **2015**, *91*, 518−526.
(28) Crine, J. P.; Yelon, A. Photogeneration and transport of carriers in atactic polystyrene. *J. Appl. Phys.* **1980**, *51*, 2106−2114.
(29) Mansour, A. .F.; El-Shaarawy, M. G.; El-Bashir, S. .M.; El-Mansy, M. K.; Hammam, M. Optical study of perylene dye doped poly(methyl methacrylate) as fluorescent solar collector. *Polym. Int.* **2002**, *51*, 393−397.
(30) Laskarakis, A.; Gravalidis, C.; Logothetidis, S. FTIR and Vis−FUV real time spectroscopic ellipsometry studies of polymer surface modifications during ion beam bombardment. *Nucl. Instrum. Methods Phys. Res., Sect. B* **2004**, *216*, 131−136.
(31) Chen, D.; Liu, Y.; Xia, C.; Han, Y.; Sun, Q.; Wang, X.; Chen, W.; Jian, X.; Lv, W.; Ma, J.; He, W. Polybenzimidazole functionalized electrolyte with Li-wetting and self-fluorination functionalities for practical Li metal batteries. *InfoMat* **2022**, *4*, No. e12247.
(32) Rad, A. S.; Nasimi, N.; Jafari, M.; Shabestari, D. S.; Gerami, E. Ab-initio study of interaction of some atmospheric gases (SO_2, NH_3, H_2O, CO, CH_4 and CO_2) with polypyrrole (3PPy) gas sensor: DFT calculations. *Sens. Actuators, B* **2015**, *220*, 641−651.
(33) Mandu, L. O.; Batagin-Neto, A. Chemical sensors based on N-substituted polyaniline derivatives: reactivity and adsorption studies via electronic structure calculations. *J. Mol. Model.* **2018**, *24*, 157.
(34) Ullah, H.; Ayub, K.; Ullah, Z.; Hanif, M.; Nawaz, R.; Shah, A. u. H. A.; Bilal, S.; Bilal, S. Theoretical insight of polypyrrole ammonia gas sensor. *Synth. Met.* **2013**, *172*, 14−20.

https://doi.org/10.1021/acsphyschemau.3c00025
ACS Phys. Chem Au 2023, 3, 521−531